Accurate Global Potential Energy Surface and Reaction Dynamics for the Ground State of $HgBr_2$

Nikolai B. Balabanov,† Benjamin C. Shepler,‡ and Kirk A. Peterson*

Department of Chemistry, Washington State University, Pullman, Washington 99164-4630

Received: June 23, 2005; In Final Form: July 29, 2005

A global potential energy surface (PES) for the $^1A'$ ground state of $HgBr_2$ has been constructed in order to determine the rate constants for atmospherically important reactions involving mercury and bromine. The total energy of $HgBr_2$ was calculated by the multireference configuration interaction level of theory with series of correlation consistent basis sets up to quadruple-ζ quality with subsequent extrapolation to the complete basis set limit. An additive correction for spin−orbit coupling was also included. The global PES was represented piecewise by interpolating three separate parts of the surface with the reproducing kernel Hilbert space method and connecting them smoothly by switch functions. Quasiclassical trajectory calculations carried out on the surface yielded 298 K thermal rate constants of 3.89×10^{-11} cm^3/(mol·s) for the abstraction reaction HgBr + Br → Hg + Br_2, 2.98×10^{-11} cm^3/(mol·s) for the recombination reaction Br + HgBr → $HgBr_2$, and 3.97×10^{-11} cm^3/(mol·s) for the exchange reaction Br + HgBr → BrHg + Br. The insertion reaction Hg + Br_2 → $HgBr_2$ was found to have a high barrier of 27.2 kcal/mol and a very small rate constant of just 2.74×10^{-31} cm^3/(mol·s) determined by the microcanonical variational transition state theory method. The implications of the obtained results to the description of the mechanism of recently observed polar tropospheric mercury depletion events are briefly discussed.

I. Introduction

The contamination of remote polar regions, which are generally thought to be ecologically safe, has been of growing concern due to the recent discovery of mercury depletion events[1] (MDEs). These periodic rapid depletions of atmospheric gaseous mercury (predominantly in elemental Hg^0 form) were observed in both the Arctic[1,2] and Antarctic[3,4] during polar springtime. The periods of nearly complete removal of mercury from the atmosphere is always accompanied by an increase in concentration of mercury compounds on snow and ice surfaces.[2,5,6] It was also observed[1] that MDEs mimic the analogous depletions of ozone[7] occurring at the polar regions in this same period of time. Since there is strong evidence that ozone depletions are due to its reaction with halogen radicals generated photochemically from sea salts after polar sunrise,[8] the oxidation of elemental mercury by halogen radicals is also considered to be one of the major mechanisms for MDEs.[2,5,9,10] The reactions of elemental gaseous mercury and halogens probably produce what are called reactive gaseous mercury (RGM) species that apparently quickly deposit on snow and ice packs.[2,5,9,10]

One of the most likely reactions that can occur during the MDEs is oxidation of elemental mercury by bromine radicals. This might be described by a set of elemental reactions such as

$$Br_2 + h\nu \rightarrow 2Br \quad (1)$$

$$Hg + Br \rightarrow HgBr \quad (2)$$

$$HgBr + Br \rightarrow HgBr_2 \quad (3)$$

where $HgBr_2$ is one of the most probable RGM species that might deposit on the surface. Of course, the bimolecular reaction 3 might also be accompanied by abstraction of a bromine atom

$$HgBr + Br \rightarrow Hg + Br_2 \quad (4)$$

or by the exchange of the bromine atom

$$HgBr(1) + Br(2) \rightarrow Br(1) + HgBr(2) \quad (5)$$

Theoretically the RGM species $HgBr_2$ can also be produced via a direct insertion reaction of the mercury atom into the Br_2 bond

$$Hg + Br_2 \rightarrow HgBr_2 \quad (6)$$

The main focus of the present paper is on the high level theoretical determination of the rate constants of reactions 3−6. For this purpose an accurate ab initio global potential energy surface (PES) of $HgBr_2$ was constructed and the reaction rate constants were then evaluated with use of quasiclassical trajectory (QCT) calculations or by variational transition state theory (VTST). Reaction 2, which is the prerequisite for reactions 3−5, will be carefully examined in another publication.[11] The details of the ab initio electronic structure calculations are described in section II, those of construction of the global potential surface of $HgBr_2$ are given in section III, the description of the calculations of the rate constants can be found in section IV, and the comparison of the obtained results with known experimental[12] and previous theoretical[13] data on the rate constants of reactions 3 and 6 and the discussion of their atmospheric implications is presented in section V. The conclusions drawn from the present work are summarized in section VI.

II. Details of the Ab Initio Calculations

In the electronic structure calculations the Br 1s−2p and Hg 1s−4f electrons were described by relativistic small core

* Corresponding author. E-mail: kipeters@wsu.edu.
† E-mail: nick@mail.wsu.edu.
‡ E-mail: bshepler@wsu.edu.

10.1021/jp053415l CCC: $30.25
Published on Web 09/13/2005

pseudopotentials of the Stuttgart-Köln type.[14,15] The remaining Br (3s3p3d4s4p) and Hg (5s5p5d6s) electrons were explicitly treated with series of augmented correlation consistent basis sets, aug-cc-pV*n*Z-PP, constructed for use with these pseudopotentials.[14,16] The quality of basis sets ranged from double-ζ to quadruple-ζ (n = D, T, Q) and only the pure spherical d-, f-, g-, and h-type angular momentum functions were employed in the calculations. The total number of basis functions for the $HgBr_2$ system consisted of 118 for double-ζ, 198 for triple-ζ, and 313 for the quadruple-ζ calculations. All calculations were performed in C_s effective symmetry.

The total energies of the $HgBr_2$ ground electronic state were calculated by the internally contracted multireference configuration interaction (singles and doubles) method[17,18] with the multireference Davidson correction for an approximate treatment of the effect of higher excitations[19−21] (icMRCI+Q). The orbitals for the icMRCI+Q calculations were determined by the state-averaged complete active space self-consistent field (CASSCF) method by averaging four lowest $^1A'$ and two lowest $^3A'$ electronic states with equal weights. The active space in these CASSCF calculations consisted of eight molecular orbitals originating from the Hg 6s, $6p_x$, $6p_y$, $6p_z$ and Br $4p_x$, $4p_z$ AOs (assuming $HgBr_2$ is lying in the xz plane). The Hg 5d and Br 4s, $4p_y$ were always kept doubly occupied in the CASSCF procedure. The CASSCF wave function consisted of 980 configuration state functions (CSFs) for singlet states and 1176 CSFs for triplet states. This choice of active space and number of states included in the averaging procedure allowed us to obtain well-defined molecular orbitals over different regions of the $HgBr_2$ potential energy surface.

In the icMRCI+Q calculations, the active space consisted of orbitals arising from Hg 5d, 6s, and 6p and Br 4p AOs. The CSFs in the reference space were generated with the restrictions that the Hg 5d and Br $4p_y$ orbitals were doubly occupied and the Hg $6p_x$, $6p_y$, and $6p_z$ orbitals had a maximum occupation of a single electron in any one CSF. When used with the aug-cc-pVQZ-PP basis, the largest basis set employed in this work, the icMRCI wave function consisted of about 8.5 million variational parameters, which effectively took into account more than 327 million uncontracted CSFs. All CASSCF and icMRCI+Q calculations described above were carried out with the MOLPRO suite[22] of quantum chemistry programs.

After calculating the icMRCI+Q energy with each basis set (DZ, TZ, QZ), the complete basis set limits of the icMRCI+Q total energies were then obtained by averaging the CBS limits found by two extrapolations: a mixed exponential and Gaussian form[23]

$$E_n = E_{CBS} + A\mathrm{e}^{-(n-1)} + B\mathrm{e}^{-(n-1)^2} \tag{7}$$

using n = 2 (DZ), 3 (TZ), and 4 (QZ) and a 2-point n^{-3} formula[24−26]

$$E_n = E_{CBS} + \frac{A}{n^3} \tag{8}$$

which utilized energies for n = 3 (TZ) and 4 (QZ). Total energies were used in both cases.

Finally, corrections for the spin-obit interaction, ΔE_{SO}, were added to the icMRCI+Q/CBS energies. ΔE_{SO} was obtained as the difference in energy of the lowest spin−orbit state and the energy of the lowest singlet state of $HgBr_2$. The spin−orbit energy was obtained by the spin−orbit MRCI method[27] taking into account only single electron excitations (SO-MRCIS) with the aug-cc-pVTZ-PP basis sets. The energy of the lowest singlet state was found with the same method, but without the SO interaction. Both these calculations were carried out with the COLUMBUS package,[28−31] but utilized the orbitals obtained in the MOLPRO CASSCF calculations as described above. The active space in the (SO-) MRCIS work consisted of the Hg 6s5d and Br 4s4p orbitals. In the spin−orbit calculations the effective spin−orbit potentials that are part of the relativistic core potentials on Br[14] and Hg[15] were used, and the wave function was constructed with the inclusion of both singlet and triplet CSFs.

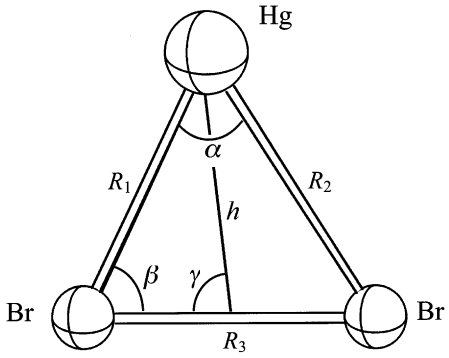

Figure 1. Notation of coordinates for $HgBr_2$ used in sampling and fitting the PES.

III. Construction of an Analytical PES

A. Sampling. The potential energy surface of $HgBr_2$ was divided into three regions corresponding to the abstraction reaction HgBr + Br → Hg + Br_2, insertion reaction Hg + Br_2 → $HgBr_2$, and recombination reaction Br + HgBr → $HgBr_2$. Each of these sections was sampled by a regular three-dimensional grid in its natural internal coordinates. The definition of the internal coordinates R_1, R_2, R_3, h, α, β, and γ are shown in Figure 1; i.e., R_1 and R_2 are the two HgBr distances, R_3 is the BrBr distance, h is the distance from the Hg atom to the center of mass (CM) of Br_2, α is the valence angle Br−Hg−Br, β is the larger of the two Hg−Br−Br valence angles, and γ is the smaller of the two Br−CM−Hg angles.

For the recombination reaction part of the surface, the internal coordinates were R_1, R_2, and α. A grid of 1296 configurations was generated by choosing R_1 and R_2 to be {3.5, 3.7, 3.9, 4.05, 4.2, 4.35, 4.50, 4.65, 4.8, 4.95, 5.15, 5.4, 6.0, 7.0, 8.5, 10.0, 15.0, and 30.0}a_0, and α to be {179.9, 160, 140, and 120}°. However the icMRCI+Q/CBS + Δ*SO* energies were calculated only for the 420 symmetry unique points with both R_1 and R_2 ≥ $4.2a_0$. The energies for shorter distances were explicitly determined only at the icMRCI+Q/aug-cc-pVTZ-PP level of theory and only for α = 179.9°. The final energies $E(X_1, X_2, \alpha)$ for the points with $X_1(=R_1)$ or $X_2(=R_2) \le 4.05a_0$ were then estimated by first calculating the factor ξ, which is independent of α

$$\xi = \frac{E^{TZ}(X_1,X_2) - E^{TZ}(R_1^*,R_2^*)}{E^{TZ}(R_1,R_2) - E^{TZ}(R_1^*,R_2^*)} \tag{9a}$$

where (R_1,R_2) is a point on the edge of the rectangle [4.2:30.0] × [4.2:30.0] closest to (X_1,X_2) and (R_1^*, R_2^*) is the analogous point on the edge of the rectangle [4.35:30.0] × [4.35:30.0], each at α = 179.9°. The value of $E(X_1,X_2, \alpha)$ was then obtained by

$$E(X_1,X_2,\alpha) = E(R_1^*,R_2^*,\alpha) + \xi[E(R_1,R_2,\alpha) - E(R_1^*,R_2^*,\alpha)] \quad (9b)$$

It should be stressed that this particular extrapolation procedure mainly accounted for the basis set dependence of these short range data points since all of the collinear points were explicitly calculated with the aug-cc-pVTZ-PP basis set. In particular, these points had relatively high energies and were only necessary to include in the final fit to improve the behavior of the RKHS interpolation at short range.

For the abstraction reaction, the natural internal coordinates are R_1, R_3, and β. The R_1 distance ran over the array {4.2, 4.4, 4.6, 4.8, 5.0, 5.3, 6.0, 7.5, 9.0, 13.0, and 25.0}a_0, R_3 distances were chosen from {4.1, 4.3, 4.5, 4.7, 5.0, 5.3, 6.0, 7.5, 9.0, 13.0, and 25.0}a_0, and β = {179.9, 160, 140, and 120}°, which gave 484 geometries.

The points for the insertion reaction region were sampled in Jacobi coordinates h, R_3, and γ. The values for the median h were chosen from {3.0, 4.0, 4.5, 5.0, 5.5, 6.0, 7.0, 8.0, 10.0, and 15.0}a_0, the R_3 distance ran over {4.0, 5.0, 5.5, 6.0, 6.5, 7.0, 8.0, 9.5, 13.0, and 20.0}a_0, and the angle γ was selected from {45, 60, 75, 90}°, which resulted in 400 symmetry-unique points.

To describe the two-body interaction of the Hg and Br atoms, calculations were carried out for the $HgBr_2$ molecule with one of the Hg−Br distances always kept at $50a_0$. The values of the other Hg−Br distance were chosen from {3.2, 3.4, 3.6, 3.8, 4.0, 4.1, 4.2, 4.4, 4.5, 4.6, 4.7, 4.8, 4.9, 5.0, 5.2, 5.7, 6.3, 7.0, 8.0, 9.0, 10.0, 11.0, 13.0, 15.0, and 30}a_0. The points corresponding to distances $\geq 4.0a_0$ were explicitly calculated at the icMRCI+Q/CBS + ΔSO level, while the remaining points in the short distance region were obtained by extrapolation via the exponential function $A + B\exp(-R) + C\exp(-2R)$. The coefficients in the latter equation were obtained by fitting to the shortest three data points. Similar calculations were performed to obtain energies of the Br−Br diatom interaction. The Br−Br distance was sampled from {2.9, 3.1, 3.3, 3.5, 3.7, 3.9, 4.0, 4.1, 4.2, 4.3, 4.4, 4.5, 4.6, 4.7, 4.9, 5.3, 6.0, 7.0, 8.5, 10.0, 13.0, and 30.0}a_0. The energies for the five shortest distances were obtained by exponential extrapolation as in Hg−Br.

Finally, a small grid was also sampled around the near-equilibrium geometry of $HgBr_2$ to improve the analytical representation of the PES in this region. A total of 22 points (14 symmetry unique) were sampled in (R_1, R_2, α) internal coordinates in the range $4.41-4.81a_0$ for distances and 160−180° for the valence angle α.

B. Fitting. The data of regular grids for the recombination, abstraction, and insertion reaction regions were first decomposed using the general many-body expansion,[32] i.e.

$$\tilde{V}(R_1,R_2,R_3) = V^{(1)} + V^{(2)}_{HgBr}(R_1) + V^{(2)}_{HgBr}(R_2) + V^{(2)}_{BrBr}(R_3) + V^{(3)}(R_1,R_2,R_3) \quad (10)$$

where $V^{(1)}$ is the sum of energies of two separated Br atoms and the Hg atom, $V^{(2)}$ is the energy of the two-body interaction of the corresponding pair of atoms, and $V^{(3)}$ is the three-body interaction energy.

Diatomic interaction terms $V^{(2)}$ were interpolated via the one-dimensional reproducing kernel Hilbert space method[33] (RKHS)

$$V^{(2)}(R) = \sum_{i=1}^{n} C_i q(R,R^i) \quad (11)$$

where q is a distancelike reproducing kernel[33]

$$q(x,x') = \frac{1}{14} x_>^{-7}\left\{1 - \frac{7}{9}\frac{x_<}{x_>}\right\} \quad (12)$$

and $x_< = \min(x,x')$ and $x_> = \max(x,x')$.

The regular grids of three-body energies for abstraction, recombination, and insertion on the global PES were interpolated separately with the multidimensional RKHS formula[33]

$$V^{(3)}_{region}(S_1,S_2,S_3) = \sum_{i,j,k=1}^{n_1,n_2,n_3} C_{ijk} q_1(S_1,S_1^i) q_2(S_2,S_2^j) q_3(S_3,S_3^k) \quad (13)$$

where S_i and q_i (i = 1, 2, 3) are fitting coordinates and one-dimensional reproducing kernels, respectively, that are appropriate for each region. For the recombination and abstraction regions, kernels q_1 and q_2 in eq 13 were distancelike reproducing kernels given by eq 12, while q_3 was an anglelike reproducing kernel[33]

$$q(x,x') = 1 + x_< x_> + 2x_<^2 x_>\left\{1 - \frac{1}{3}\frac{x_<}{x_>}\right\} \quad (14)$$

The fitting coordinates for the recombination piece were chosen to be

$$S_1 = 1 - \exp(-aR_1)$$
$$S_2 = 1 - \exp(-aR_2)$$
$$S_3 = \frac{1}{2}(1 + \cos\alpha) \quad (15)$$

and for the abstraction piece, the corresponding coordinates were

$$S_1 = 1 - \exp(-aR_1)$$
$$S_2 = 1 - \exp(-aR_2)$$
$$S_3 = \frac{1}{2}(1 + \cos\beta) \quad (16)$$

where $a > 0$ was a parameter (∼0.1). It was found that the use of exponential coordinates S_1 and S_2 of form (15) and (16) instead of the original R_1, R_2, and R_3 distances in the RKHS formula (13) produced significantly smaller C_{ijk} coefficients.

For the insertion reaction piece, the q_1 kernel in eq 13 was a Taylor spline reproducing kernel[34]

$$q(x,x') = 2x_<^2 x_>\left\{1 - \frac{1}{3}\frac{x_<}{x_>}\right\} \quad (17)$$

q_2 was a distancelike kernel (eq 12), and q_3 was an anglelike kernel (eq 14). The fitting coordinates for the insertion region were chosen as

$$S_1 = \cosh^{-1}(bh)$$
$$S_2 = 1 - \exp(-aR_3)$$
$$S_3 = \sin^2\gamma \quad (18)$$

where b was a parameter (∼0.25). The use of the inverse hyperbolic cosine function for the description of the median h is dictated by the properties of the three-body potential of $HgBr_2$: it is an even function relative to the h coordinate, vanishes when $h \rightarrow \infty$, and has a minimum or maximum at h=0.

The three functions of the form of eq 13 for the insertion, abstraction, and recombination reaction regions were then combined into one global surface via the relation

$$V^{(3)} = \chi(R_1,R_2,R_3)[\Omega_+(\beta;\beta',\kappa_\beta)V^{(3)}_{abs} + \Omega_-(\beta;\beta',\kappa_\beta) \times \{\Omega_+(\alpha;\alpha',\kappa_\alpha)V^{(3)}_{ins} + \Omega_-(\alpha;\alpha',\kappa_\alpha)V^{(3)}_{rec}\}] \quad (19)$$

where

$$\Omega_\pm(\phi;\phi',\kappa) = \frac{1}{2}[1 \pm \tanh(\kappa(\phi - \phi'))] \quad (20)$$

is a pair of functions for a smooth switch[35] between the intervals $(-\infty,\phi']$ and $[\phi',\infty)$. It is worthwhile to note that $\Omega_+ + \Omega_- \equiv 1$ and parameter κ controls the strength of the switch. The values for the parameters were accepted as follows: $\alpha' = 115°$, $\beta' = 115°$, $\kappa_\alpha = 0.3$, and $\kappa_\beta = 0.3$. The χ function in eq 19 is designed to vanish at long range and is described in terms of switch functions (eq 20) as

$$\chi(R_1,R_2,R_3) = \prod_{i=1}^{3}\Omega_+(R_i;R_i',\kappa_R) \quad (21)$$

where $R_i' = 15.0a_0$ and $\kappa_R = 0.5$. The χ term is introduced in order to equivalence the long distance parts of the three-body terms obtained through interpolation of the three separate grids.

The small grid sampled around the near-equilibrium geometry of $HgBr_2$ was fitted with a polynomial function of the form

$$V_{eq}(Q_1,Q_2,Q_3) = \sum_{i,j,k} C_{ijk}(Q_1)^i(Q_2)^j(Q_3)^k \quad (22)$$

where the coordinates Q_i were

$$Q_1 = R_1 - R_{1e}$$
$$Q_2 = R_2 - R_{2e}$$
$$Q_3 = \alpha - 180° \quad (23)$$

The SURFIT program[36] was used to obtain the equilibrium distances (R_{1e}, R_{2e}) and the C_{ijk} coefficients in eq 22.

The final global $HgBr_2$ potential energy surface was then described by the formula

$$V(R_1,R_2,R_3) = \Omega_+(\rho;\rho',\kappa_\rho)V_{eq}(R_1,R_2,R_3) + \Omega_-(\rho;\rho',\kappa_\rho)\tilde{V}(R_1,R_2,R_3) \quad (24)$$

where

$$\rho = \sqrt{(R_1 - R_{1e})^2 + (R_2 - R_{2e})^2 + (\alpha - 180)^2 + \lambda} \quad (25)$$

In eq 25, λ is a small parameter (0.001) introduced to avoid a discontinuity in the analytical first derivatives at the equilibrium geometry of $HgBr_2$. The values for the parameters of the switch function were chosen as $\rho' = 1$ and $\kappa_\rho = 1$.

It should be mentioned that after connecting different parts into one global surface, the final analytical function does not exactly interpolate all of the original data. However, nearly all of the significant errors are located at very high energies on the repulsive wall, and all the data around the minimum energy paths for reactions 3−6 are accurately reproduced by the fit. The overall root-mean-square error of the final fit relative to the original data (2202 total points, 1069 symmetry unique) was just 0.12 kcal/mol. It should also be noted that the RKHS formula (eq 13) was never directly used to compute the three-body potential energies in our calculations. Instead the fast algorithm for evaluation of the RKHS surface as described in ref 37 was employed. Switching to the fast summation technique resulted in speeding up the evaluation of the potential energy and its analytical partial derivatives by a factor of ∼10 for the insertion and abstraction regions and up to 17 times for the recombination part. This significantly decreased the time for running trajectories. The code that computes the $HgBr_2$ potential energy and its gradient was interfaced to the POLYRATE[38] and VENUS96[39] dynamics programs using the POTLIB2001[40] utility package and is available upon request from the authors.

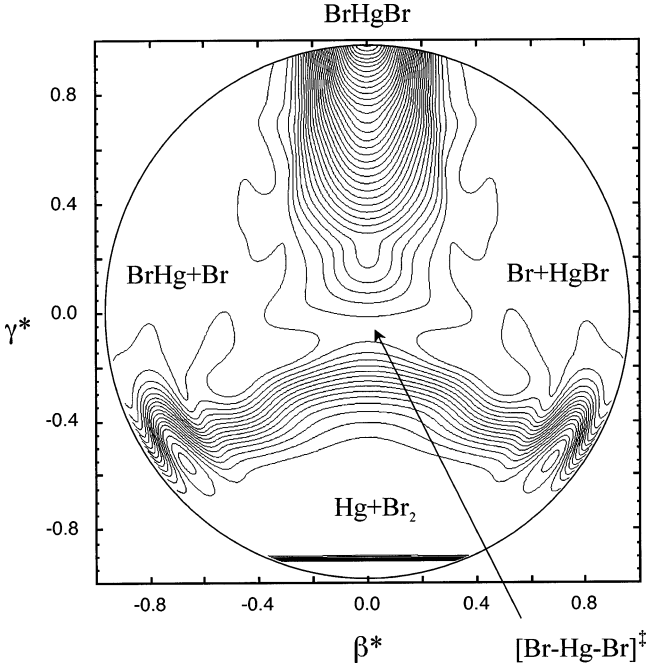

Figure 2. Relaxed triangle equipotential contour plot of the $HgBr_2$ PES given relative to the Br + Hg+Br energy in kcal/mol. Contours are equally spaced by 2 starting at −90 and finishing at −15. The plot is shown in the coordinates $\beta^* = \sqrt{3}(R_1^2 - R_2^2)/Q$ and $\gamma^* = (2R_3^2 - R_1^2 - R_2^2)/Q$, where $Q = R_1^2 + R_2^2 + R_3^2$ is varied to minimize the potential energy at the given point (β^*,γ^*), where $(\beta^*)^2+(\gamma^*)^2 \le 1$. Notations of the coordinates R_1, R_2, R_3 are found in Figure 1. At the transition state $\beta^* = 0$ and $\gamma^* = -0.135$.

C. Characteristics of the Analytical PES. Figure 2 presents a relaxed triangle plot[41] of the $HgBr_2$ potential energy surface using hyperspherical-like symmetrical coordinates.[42] More detailed plots of the insertion, abstraction, and recombination reactions in their natural coordinates are shown in Figures 3−5, respectively. In general the surface features two symmetrical valleys corresponding to the HgBr + Br → Hg + Br_2 abstraction reaction(s), a van der Waals well along the minimum energy path (MEP) of the abstraction reaction, a global minimum corresponding to the linear Br−Hg−Br insertion complex, and a saddle point corresponding to the barrier for the insertion reaction Hg + Br_2 → $HgBr_2$. The geometrical configuration of the saddle point is symmetrical with R_1(Hg−Br) = R_2(Hg−Br) = 2.853 Å and α(Br−Hg−Br) = 55.74°. The barrier for the insertion reaction 6 obtained from the present PES is 27.2 kcal/mol relative to the energy of the Hg+Br_2 reactants. Both reaction 4 for abstraction of the bromine atom from HgBr and the recombination reaction 3 to linear Br−Hg−Br are barrierless, and the corresponding MEPs go through linear geometrical configurations. The van der Waals minimum along the abstraction reaction MEP is located at R_1(Hg−Br) = 3.138 Å and R_3-(Br−Br) = 2.307 Å with a binding energy for the Hg−Br_2 adduct of 1.97 kcal/mol. Additional calibration calculations at

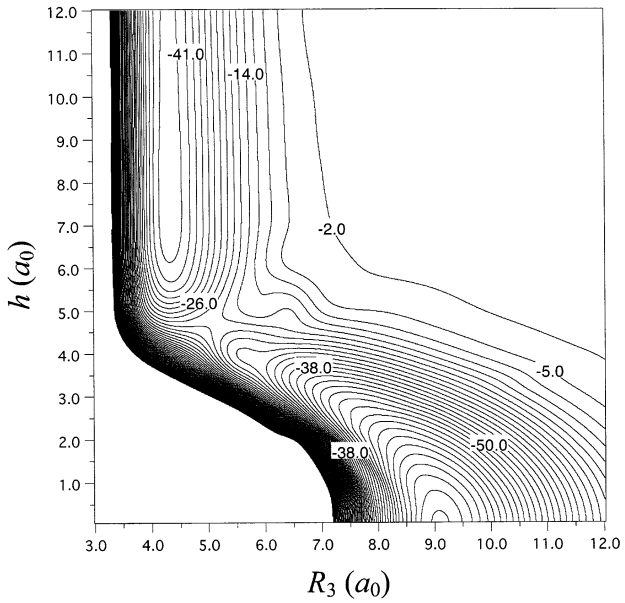

Figure 3. Equipotential contour plot of the $HgBr_2$ PES for fixed $\gamma = 90°$ in (h,R_2,γ) Jacobi coordinates (Hg + Br_2 insertion reaction). The contours are equally spaced by 2 kcal/mol; the total energy is relative to completely separated ground-state atoms.

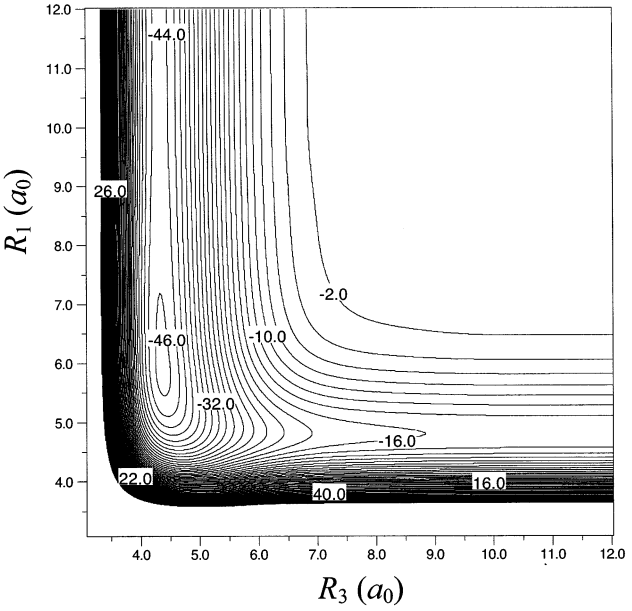

Figure 4. Equipotential contour plot of the $HgBr_2$ PES for fixed $\beta = 180°$ in (R_1,R_3,β) valence coordinates (Hg + Br_2 abstraction reaction). The contours are equally spaced by 2 kcal/mol; the total energy is relative to completely separated ground-state atoms.

the CCSD(T)/CBS level of theory using DZ through QZ basis sets indicate that this binding energy is too small at this level of theory by only about 0.6 kcal/mol. The van der Waals interaction energy of Hg and Br_2 is comparable to the value of 1.34 kcal/mol for the Hg−I_2 complex determined in a crossed beam study of the rainbow scattering of Hg by I_2 by Wilcomb et al.[43]

To evaluate the accuracy of the constructed $HgBr_2$ global potential surface, we performed an analysis of the stationary points and asymptotes with the POLYRATE program in order to compare their structures and energies to the results of our previous accurate ab initio calculations[44,45] of the thermochemistry and structures of mercury bromides and/or available experimental data. The results are given in Tables 1 and 2. The

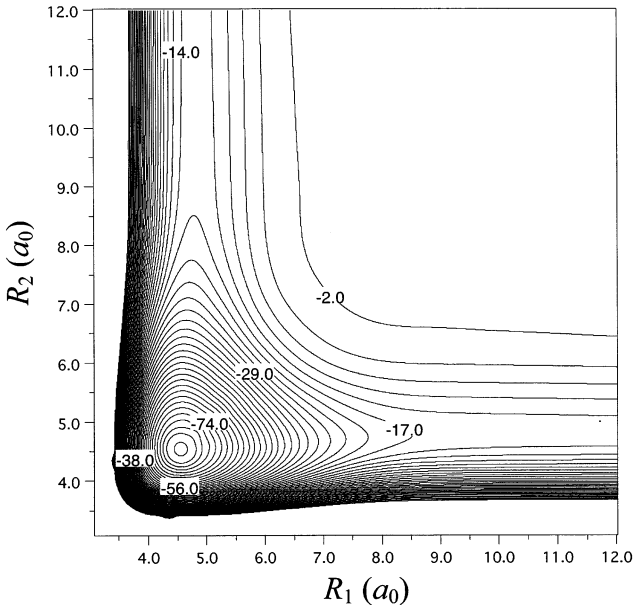

Figure 5. Equipotential contour plot of the $HgBr_2$ PES for fixed $\alpha = 180°$ in (R_1,R_2,α) valence coordinates (HgBr + Br recombination reaction). The contours are equally spaced by 3 kcal/mol; the total energy is relative to completely separated ground-state atoms.

TABLE 1: Equilibrium Structures (R, Å) and Harmonic Frequencies (ω_i, cm^{-1}) at Stationary Points and Asymptotes on the IcMRCI+Q/CBS+SO Potential Energy Surface of $HgBr_2$

point	parameter	current surface	best estimate
Hg + Br_2	R_e(BrBr)	2.288	2.281[a]
	ω_e	325.0	325.31[a]
HgBr + Br	R_e(HgBr)	2.544	2.527[b]
	ω_e	185.8	188.25[c]
$HgBr_2$ (min)	R_e(HgBr)	2.404	2.377[d]
	ω_1 (Σ^+)	231.6	226.9[d]
	ω_2 (Π)	71.6	69.6[d]
	ω_3 (Σ^-)	302.5	297.8[d]
Hg−Br_2 (TS)	R_e(HgBr)	2.853	
	α(BrHgBr)	55.74	
	ω_1 (A_1)	152.6	
	ω_2 (A_1)	189.4i	
	ω_3 (B_2)	55.7	

[a] Reference 62. [b] Reference 44. [c] Reference 63. [d] Reference 45.

TABLE 2: Heats of Reactions ΔH_r(0K), Kcal/Mol

reaction	current surface	best previous theoretical result[a]	experiment[b]
HgBr + Br → Hg + Br_2	−28.9	−30.6	−29.91 ± 0.37
HgBr + Br → $HgBr_2$	−73.4	−72.4	−72.33 ± 2.34
Hg + Br_2 → $HgBr_2$	−44.4	−42.4	−42.42 ± 2.05

[a] Reference 44. [b] Using ΔH_f(0K) = 15.42 ± 0.01 kcal/mol for Hg, ΔH_f(0K) = 28.18 ± 0.01 kcal/mol for Br, ΔH_f(0K) = 10.92 ± 0.03 kcal/mol for Br_2, and ΔH_f(0K) = −16.08 ± 2.01 kcal/mol for $HgBr_2$ from JANAF data.[64] An experimental ΔH_f(0K) = 28.07 ± 0.34 kcal/mol for HgBr was calculated using the D_0(HgBr) = 15.53±0.32 kcal/mol from ref 65.

current surface accurately reproduces the equilibrium BrBr distance and harmonic frequency of Br_2 and the harmonic frequencies in the HgBr and $HgBr_2$ molecules. The equilibrium HgBr distances in both HgBr and $HgBr_2$, however, are somewhat longer by ∼0.03 Å than those obtained previously[44,45] by the CCSD(T) method. These differences cannot be explained by just the neglect of core-valence correlation effects in the present study, since according to our previous work the core-valence effect on the HgBr distance in $HgBr_2$ consists of just

0.009 Å. Therefore, the reason for the discrepancies is mostly due to differences in the treatment of electron correlation by the icMRCI+Q method used in the present study compared to the CCSD(T) method used previously.[44,45] Apparently, the icMRCI+Q method of this work does not recover as much electron correlation around the single determinant dominated regions of the $HgBr_2$ molecule as compared to the CCSD(T) method.

The enthalpy of the insertion reaction calculated from the current PES is at the lower end of the uncertainty interval of the corresponding experimental value and 2.0 kcal/mol lower than the accurate CCSD(T) value obtained in our previous work.[44] The icMRCI+Q/CBS+SO enthalpies for abstraction and recombination are in very good agreement with the experimental enthalpies and differ by less than 1 kcal/mol from the accurate theoretical values obtained in our previous study.[44] Generally, the global potential energy surface of $HgBr_2$ constructed in the present work reproduces the best estimates for the energies and spectroscopic parameters of the species involved in these reactions, and we believe it to be very suitable for an accurate investigation of the dynamics of reactions 3−6.

IV. Details of Rate Constant Calculations

The thermal rate constants of the reactions HgBr + Br → *products* were determined by the QCT method. There are several schemes for investigation of reaction rates using the QCT approach and a general description of the QCT methodology can be found in the literature (cf., ref 46). In the present study the thermal rate constants were determined by

$$k(T) = \sum_{v,j} k^{vj}(T) \frac{(2j+1)\exp\{-E_{vj}/k_B T\}}{Q_{vr}(T)} \qquad (26)$$

where Q_{vr} is the rovibrational partition function and E_{vj} is the HgBr rovibrational energy for vibrational and rotational quantum numbers v and j found by the standard formula

$$E_{vj} = \omega_e\left(v+\frac{1}{2}\right) - \omega_e x_e\left(v+\frac{1}{2}\right)^2 + B_e\, j(j+1) - \alpha_e\left(v+\frac{1}{2}\right)j(j+1) - D_e[j(j+1)]^2 \qquad (27)$$

where the spectroscopic constants of the HgBr molecule are $\omega_e = 186.6\ cm^{-1}$, $\omega_e x_e = 0.75\ cm^{-1}$, $B_e = 0.045925\ cm^{-1}$, $\alpha_e = 0.00032\ cm^{-1}$, and $D_e = 1.10 \times 10^{-8}\ cm^{-1}$ calculated from the two-body HgBr potential of the current work.

The reaction rates $k^{vj}(T)$ for each (v, j) rovibrational energy level were found by

$$k^{vj}(T) = g_e\left(\frac{8k_BT}{\pi\mu_{HgBr+Br}}\right)^{1/2}\sigma^{vj} \qquad (28)$$

where g_e is the electronic degeneracy number; $g_e = 1/8$ for the recombination reaction 3 and abstraction reaction 4 and $g_e = 1$ for the exchange reaction 5. In addition, k_B is the Boltzmann constant, $\mu_{HgBr+Br}$ is the reduced mass, and σ^{vj} is the reaction cross section

$$\sigma^{vj} = \pi b_{max}\frac{N_r^{vj}}{N} \qquad (29)$$

In eq 29 b_{max} is the maximum impact parameter, N_r^{vj} is the number of reactive trajectories for a given reactant (v, j) rovibrational level, and N is the total number of trajectories.

TABLE 3: Definition of Trajectory Termination Criteria for HgBr + Br

no.	product[a]	criteria[b]
1	BrHg + Br	$R_1 < 3.5$ and $R_2 > 12.0$ and $-16.0 < V < -1.0$
2	Hg + Br_2	$R_3 < 3.5$ and $h > 12.0$ and $-46.0 < V < -1.0$
3	Br + HgBr	$R_1 > 12.0$ and $R_2 < 3.5$ and $-16.0 < V < -1.0$
4	Br + Hg+Br	$R_1, R_2, R_3 > 12.0$ and $V > -1.0$
5	BrHgBr	$V < -50.0$ and *time* > 10^{-11} s

[a] Channel No. 1 corresponds to a nonreactive trajectory while channel No. 3 describes the exchange reaction. [b] Distances R_1, R_2, R_3, and h are in Å; see Figure 1 and text for the notation of coordinates. Potential energy V is in kcal/mol, given relative to the Br + Hg + Br separated energy. The test for termination started after 2.5×10^{-12} s. See text for more details.

With a probability of 95%, the statistical error of the rate constants k^{vj} does not exceed

$$\Delta k^{vj} = 2k^{vj}\left[\frac{(N - N_r^{vj})}{NN_r^{vj}}\right]^{1/2} \qquad (30)$$

The sum of the Δk^{vj} values analogous to eq 26 gives then the estimate to the total error $\Delta k(T)$ of the rate constant $k(T)$.

The QCT calculations were carried out with the VENUS96 program.[39] The initial translational energies were generated by sampling a Maxwell−Boltzmann distribution, and the maximum impact parameter $b_{max} = 9.0$ Å was found in trial calculations for the $(v = 0, j = 0)$ rovibrational level of HgBr. We have verified that larger values of b_{max} did not significantly alter the reaction cross sections for the higher v and j states investigated in this study. The termination of trajectories was determined by both geometrical and energy criteria for the abstraction and exchange reaction channels, and a criterion based on the time spent in the Br−Hg−Br complex well for the recombination reaction (see Table 3). The test for termination criteria was always initiated after 2.5×10^{-12} s after the start of a trajectory. The trajectory calculations were performed for HgBr vibrational quantum numbers $v = 0, 1, 2, ..., 5$ and rotational quantum numbers $j = 0, 10, 20, ..., 200$. The total number of trajectories, N, was chosen to be 10 000 for the runs with vibrational quantum numbers $v = 0$, 1, and 2, and $N = 6000$ for the remainder of the calculations. The full set of k^{vj} ($j = 0, 1, 2, ..., 200$) was obtained by fitting the function $k^{vj} = \exp(-\alpha j^2) \times \sum_{i=1}^{3} c_{ij} j^{i-1}$ to the partial data weighted by $1/\Delta k^{vj}$ in the least squares procedure. Similarly, the full set of errors Δk^{vj} was obtained by interpolation of known errors at $j = 0, 10, 20, ..., 200$ by natural cubic splines.

Because of the high barrier for the insertion Hg + Br_2 → $HgBr_2$, one could expect a very small reaction probability for this channel at $T = 298$ K. Hence the calculation of the rate constant using the QCT method would demand very large numbers of trajectories, which would be very computationally intensive. Therefore, the rate constant for the insertion reaction was calculated by canonical (CVT), improved canonical (ICVT), and microcanonical (μVT) variational transition state theory[47−53] with use of the POLYRATE program.[38] The analogous VTST calculations were also carried out for the abstraction and recombination reactions in order to compare with the QCT results.

Finally, assuming microscopic reversibility, the rate constants k_r for the reverse reactions of reactions 3, 4, and 6 were estimated from the detailed balance principle $K_{eq} = k_f/k_r$, where K_{eq} is the corresponding equilibrium constant found using the harmonic approximation with the POLYRATE program and k_f is the calculated forward rate constant for reaction 3, 4, or 6.

TABLE 4: Thermal (298 K) Reaction Rate Constants of the Present Work[a]

	reaction[b]	QCT	CVT	ICVT	μVT
A	$HgBr + Br \rightarrow Hg + Br_2$	3.89 ± 0.17 (−11)	6.15 (−11)	5.30 (−11)	4.52 (−11)
B	$HgBr + Br \rightarrow HgBr_2$	2.98 ± 0.14 (−11)	1.27 (−10)	1.22 (−10)	1.05 (−10)
C	$Hg + Br_2 \rightarrow HgBr_2$		2.76 (−31)	2.76 (−31)	2.74 (−31)
D	$BrHg + Br \rightarrow Br + HgBr$	3.97 ± 0.35 (−11)			
E	$Hg + Br_2 \rightarrow HgBr + Br$	3.4 ± 0.15 (−31)	5.4 (−31)	4.6 (−31)	3.9 (−31)
F	$HgBr_2 \rightarrow HgBr + Br$	5.5 ± 0.26 (−39)	2.4 (−38)	2.3 (−38)	2.0 (−38)
G	$HgBr_2 \rightarrow Hg + Br_2$		5.9 (−39)	5.9 (−39)	5.8 (−39)

[a] The rate constants of reactions A−E have units of $cm^3/(mol \cdot s)$, while those of the unimolecular reactions F and G have units of s^{-1}. Numbers in parentheses denote powers of 10. [b] The rate constants for the reactions E−G were calculated from the detailed balance principle using equilibrium constants of $K = 1.146839 \times 10^{20}$ for reaction A, $K = 5.407325 \times 10^{27}$ for reaction B, and $K = 4.71417 \times 10^{7}$ for reaction C.

V. Results and Discussion

The results of the calculations of rate constants at a temperature of $T = 298.15$ K are summarized in Table 4. As expected, the thermal rate constant for the insertion $Hg + Br_2 \rightarrow HgBr_2$ is very small. Three variants of variational transition state theory yielded essentially the same result of $k = 2.74 \times 10^{-31}$ $cm^3/(mol \cdot s)$. The ICVT transition state for this reaction is located slightly toward the reactants side from the insertion saddle point on the $HgBr_2$ PES at the minimum energy path coordinate $s = -0.1787 a_o$ (by definition, $s = -\infty$ at the reactants, $s = 0$ at the saddle point, and $s = \infty$ at the products), which corresponds to valence coordinates of $R_1^{\ddagger}(HgBr) = R_2^{\ddagger}(HgBr) = 2.857$ Å, and $\alpha^{\ddagger}(Br-Hg-Br) = 56.4°$.

In the case of the abstraction reaction $HgBr + Br \rightarrow Hg + Br_2$, the ICVT collinear transition state is found at $R_1^{\ddagger}(HgBr) = 2.561$ Å and $R_3^{\ddagger}(BrBr) = 3.803$ Å. The microcanonical VTST rate constant for this reaction is just slightly higher than that obtained via the QCT calculations. The ICVT collinear transition state for the recombination reaction $Br + HgBr \rightarrow HgBr_2$ is located at $R_1^{\ddagger}(HgBr) = 2.539$ and $R_2^{\ddagger}(HgBr) = 4.567$ Å. Energetically the transition state for the recombination reaction lies ~0.5 kcal/mol higher, i.e., closer to the $Br + HgBr$ reactants, than the transition state for the abstraction reaction. Correspondingly, all forms of VTST theory applied in the current study predict that the rate constant for recombination is about a factor of 2 faster than that for abstraction.

Unlike VTST, the QCT calculations predict the rate constant for the recombination reaction to be slightly slower than that for the abstraction reaction. The QCT rate constant for recombination is also 4 times less than the corresponding μVT value. To explain this larger difference in the QCT and VTST rate constants, one should take into account that the two competing channels, the recombination $Br + HgBr \rightarrow HgBr_2$ and exchange $Br + HgBr \rightarrow BrHg + Br$, both pass through the same variational transition state and are indistinguishable by VTST. In the QCT calculations, however, these two channels have been counted separately. Also, while the VTST theory predicts a high-pressure limit for the rate constant, the QCT rate constant corresponds to a low-pressure limit. A proper accounting for pressure in the QCT calculations could be carried out via introduction of a collision partner. A nonreactive interaction with a collider (Ar, N_2) would release the excess energy of trajectories in highly excited rovibrational states of $HgBr_2$ and thus increase the number of reactive trajectories trapped inside the well of the $HgBr_2$ complex. This would decrease the number of trajectories leading to the exchange reaction of the bromine atom. Consequently, after the pressure is taken into account, the rate constant will be higher for recombination, $Br + HgBr \rightarrow HgBr_2$, and lower for exchange, $Br + HgBr \rightarrow BrHg + Br$. We hope to address this issue in a future publication.[11]

The reaction of Hg with Br_2 was previously examined in the experimental kinetics study of Ariya et al.[12] that utilized cold-vapor atomic absorption spectroscopy and mass spectroscopic detection techniques. The measurements of the reaction kinetics in that work was complicated, however, due to strong surface catalysis effects on the walls of the reaction chamber, and nearly all the elemental mercury disappeared before it could be detected in the mass spectrometer. Therefore, the authors of that study[12] were only able to predict an upper limit for the $Hg + Br_2$ reaction rate, $k < (0.9 \pm 0.2) \times 10^{-16}$ $cm^3/(mol \cdot s)$. According to our theoretical calculations, the gas-phase reactions of both $Hg + Br_2 \rightarrow HgBr_2$ and $Hg + Br_2 \rightarrow HgBr + Br$ have much smaller rate constants of $k = 2.7 \times 10^{-31}$ $cm^3/(mol \cdot s)$ and $k = 3.4 \times 10^{-31}$ $cm^3/(mol \cdot s)$, respectively.

Goodsite et al.[13] has carried out a theoretical study of a number of reactions involving Hg with Br, I, and OH with use of Rice−Ramsberg−Kassel−Marcus (RRKM) theory.[54] The RRKM model utilized in ref 13 effectively accounted for pressure by including the collision of reagents with N_2 molecules. At a temperature of 298 K and a pressure of 1 atm of N_2, the RRKM rate coefficient for the recombination reaction $Br + HgBr \rightarrow HgBr_2$ was found to be $k = 2.5 \times 10^{-10}$ $cm^3/(mol \cdot s)$, which is higher than predicted in our VTST calculations (high-pressure limit) $k = 1.05 \pm 0.14 \times 10^{-10}$ $cm^3/(mol \cdot s)$. The possible reason for this inconsistency is that the RRKM calculations of ref 13 were based on equilibrium distances, vibrational frequencies, and a bond energy of $HgBr_2$ estimated at a relatively low level of theory (the B3LYP method and double-ζ basis sets), which has quite large errors compared to the high level ab initio results[44,45] and/or experimental data (see refs 44 and 45) that could lead to an inaccurate density of states in the RRKM calculations.

Since the observation of mercury depletion events,[1] the mechanism of these phenomena, specifically the chemistry of gas-phase mercury, has been addressed in a number of publications.[2,9,10,12,13,55−58] Most of the researchers agree that conversion of elemental gaseous mercury to its reactive form is mainly due to reaction with active halogen species. One of the possible reaction paths for creation of RGM is successive oxidation of mercury by halogen atoms, predominately bromine, by reactions 2 and 3. The results of the present study strongly support this mechanism. The reaction of HgBr with Br to form the RGM species $HgBr_2$ is fast, while dissociation of the $HgBr_2$ complex to either $Hg + Br_2$ or back to $HgBr + Br$ is extremely slow. However it should be noted that the recombination reaction has two competitive channels with comparable rate coefficients, i.e., abstraction of bromine atom that reintroduces mercury and molecular bromine in the atmosphere, and the exchange reaction of the bromine atom. These channels should be considered in kinetic simulations.

Another popular choice in explaining and modeling MDE mechanisms is the reaction of Hg with BrO radicals.[2,9,59,60] BrO

radicals have been shown to be produced via the ozone destruction reaction $Br + O_3 \rightarrow BrO + O_2$ in the same locations as the observation of MDEs.[2] There is a strong anti-correlation between the concentrations of mercury and BrO.[2] In a kinetic study by Raofie and Aryia,[59] the rate constant of the reaction Hg + BrO was estimated to be $10^{-15} < k < 10^{-13}$ cm^3/(mol·s). Although in the current study we investigated the global PES of $HgBr_2$, preliminary calculations in our laboratory indicate that the topology of the HgBrO PES is similar, and therefore, general conclusions from the $HgBr_2$ case should also be valid for HgBrO. The two abstraction channels Hg + BrO → HgO + Br and Hg + BrO → HgBr + O are strongly endothermic[44,61] by 50.2 and 39.5 kcal/mol, respectively, and these reactions are likely to have small rates just like the $Hg + Br_2 \rightarrow HgBr + Br$ reaction. The insertion reaction, Hg + BrO → BrHgO, is exothermic[44] by −20.2 kcal/mol; however, our preliminary calculations at the icMRCI+Q level with triple-ζ correlation consistent basis sets also shows the presence of a large barrier (∼40 kcal/mol) like in $HgBr_2$, which implies a very low reaction probability. These factors indicate that reaction of Hg with BrO might have a more complex mechanism in order to explain the high reaction rate found in the experiments. There are also alternatives for the BrO influence on mercury oxidation. For example, Calvert and Lindberg[56] suggested the following reactions involving BrO:

$$HgBr + BrO \rightarrow HgBr_2 + O \quad (31)$$

$$HgBr + BrO \rightarrow BrHgO + Br \quad (32)$$

Analogously, for Br_2 one could consider

$$HgBr + Br_2 \rightarrow HgBr_2 + Br \quad (33)$$

From the heat of formation of BrHgO ($\Delta H_f(0K) = 27.2$ kcal/mol) accurately calculated in our previous theoretical study[44] together with experimental heats of formation $\Delta H_f(0K) = 28.18$ kcal/mol for Br(g), $\Delta H_f(0K) = 58.98$ kcal/mol for O(g), $\Delta H_f(0K) = 10.92$ kcal/mol for Br_2(g), $\Delta H_f(0K) = 31.96$ kcal/mol BrO, and $\Delta H_f(0K) = -16.08$ kcal/mol for $HgBr_2$ (see ref 44 for references), the enthalpies of reactions 31−33 are −17.1, −4.7, and −26.9 kcal/mol, respectively. Preliminary calculations carried out in our group predict that reactions 31 and 33 are barrierless. It should also be mentioned that the kinetics of the reaction of Hg with Br_2/BrO could be affected by the presence of water aerosols[57] and surfaces.[12] The effects of microsolvation on the thermochemistry and reaction dynamics of the interaction of mercury with halogenated species XY (X = Br, Cl; Y = Br, Cl, O) are currently being investigated by theoretical methods in our laboratory.

VI. Conclusions

An ab initio global potential energy surface for the ground state of $HgBr_2$ was constructed. The reference points are calculated at the icMRCI+Q/CBS+SO level of theory and the surface is represented by a smooth piecewise connection of three sections interpolated by the RKHS method. The quasiclassical trajectory calculations performed on the obtained global surface show that reaction of HgBr with a Br atom has nearly the same rate at 298 K $\{k = (3.0-4.0) \times 10^{-11}$ cm^3/(mol·s)$\}$ for all three possible product channels: BrHgBr, $Hg + Br_2$ and Br + HgBr. The insertion reaction, $Hg + Br_2 \rightarrow BrHgBr$, has a large barrier and very small rate constant at 298 K of $k = 2.74 \times 10^{-31}$ cm^3/(mol·s). The results of the present study support a mechanism whereby the reaction of mercury with halogen atoms is one of the main initiating steps for atmospheric oxidation of mercury that leads to the observed depletion events in the polar troposphere. The obtained kinetic data are expected to be valuable for future kinetics studies and model simulations.

Acknowledgment. This work was partially supported by the National Science Foundation (Grant No. CHE-0111282). The authors gratefully acknowledge Prof. B. Ramachandran (Louisiana Tech University) for his help with the trajectory calculations. The authors would also like to thank Prof. R. Duchovic (Indiana Univ.—Purdue Univ. Ft. Wayne) for his help with Venus and Potlib.

References and Notes

(1) Schroeder, W. H.; Anlauf, K. G.; Barrie, L. A.; Lu, J. Y.; Steffen, A.; Schneeberger, D. R.; Berg, T. *Nature (London)* **1998**, *394*, 331.
(2) Lindberg, S. E.; Brooks, S.; Lin, C.-J.; Scott, K. J.; Landis, M. S.; Stevens, R. K.; Goodsite, M.; Richter, A. *Environ. Sci. Technol.* **2002**, *36*, 1245.
(3) Ebinghaus, R.; Kock, H. H.; Temme, C.; Einax, J. W.; Lowe, A. G.; Richter, A.; Burrows, J. P.; Schroeder, W. H. *Environ. Sci. Technol.* **2002**, *36*, 1238.
(4) Temme, C.; Einax, J. W.; Ebinghaus, R.; Schroeder, W. H. *Environ. Sci. Technol.* **2003**, *37*, 22.
(5) Steffen, A.; Schroeder, W. H.; Bottenheim, J. W.; Narayan, J.; Fuentes, J. D. *Atmos. Environ.* **2002**, *36*, 2653.
(6) Berg, T.; Sekkesaeter, S.; Steinnes, E.; Valdal, A.-K.; Wibetoe, G. *Sci. Total Environ.* **2003**, *304*, 43.
(7) Boudries, H.; Bottenheim, J. W. *Geophys. Res. Lett.* **2000**, *27* (4), 517.
(8) Oltmans, S. J.; Schnell, R. C.; Sheridan, P. J.; Peterson, R. E.; Li, S.-M.; Winchester, J. W.; Tans, P. P.; Sturges, W. T.; Kahl, J. D.; Barrie, L. A. *Atmos. Environ.* **1988**, *23*, 2431.
(9) Ariya, P. A.; Dastoor, A. P.; Amyot, M.; Schroeder, W. H.; Barrie, L.; Anlauf, K.; Raofie, F.; Ryzhkov, A.; Davignon, D.; Lalonde, J.; Steffen, A. *Tellus B* **2004**, *56B* (5), 397.
(10) Skov, H.; Christensen, J. H.; Goodsite, M. E.; Heidam, N. Z.; Jensen, B.; Wahlin, P.; Geernaert, G. *Environ. Sci. Technol.* **2004**, *38*, 2373.
(11) Shepler, B. C.; Peterson, K. A. *in preparation.*
(12) Ariya, P. A.; Khalizov, A.; Gidas, A. *J. Phys. Chem. A* **2002**, *106*, 7310.
(13) Goodsite, M. E.; Plane, J. M. C.; Skov, H. *Environ. Sci. Technol.* **2004**, *38*, 1772.
(14) Peterson, K. A.; Figgen, D.; Goll, E.; Stoll, H.; Dolg, M. *J. Chem. Phys.* **2003**, *119*, 11113.
(15) Figgen, D.; Rauhut, G.; Dolg, M.; Stoll, H. *Chem. Phys.* **2005**, *311* (1−2), 227.
(16) Peterson, K. A.; Puzzarini, C. *Theor. Chem. Acc.* **2005**, in press.
(17) Knowles, P. J.; Werner, H.-J. *Chem. Phys. Lett.* **1988**, *145* (6), 514.
(18) Werner, H.-J.; Knowles, P. J. *J. Chem. Phys.* **1988**, *89*, 5803.
(19) Langhoff, S. R.; Davidson, E. R. *Int. J. Quantum Chem.* **1974**, *8*, 61.
(20) Blomberg, M. R. A.; Siegbahn, P. E. M. *J. Chem. Phys.* **1983**, *78*, 5682.
(21) Simons, J. *J. Phys. Chem.* **1989**, *93*, 626.
(22) MOLPRO, a package of ab initio programs designed by Werner, H.-J.; Knowles, P. J. version 2002.6. Amos, R. D.; Bernhardsson, A.; Berning, A.; Celani, P.; Cooper, D. L.; Deegan, M. J. O.; Dobbyn, A. J.; Eckert, F.; Hampel, C.; Hetzer, G.; Knowles, P. J.; Korona, T.; Lindh, R.; Lloyd, A. W.; McNicholas, S. J.; Manby, F. R.; Meyer, W.; Mura, M. E.; Nicklass, A.; Palmieri, P.; Pitzer, R.; Rauhut, G.; Schütz, M.; Schumann, U.; Stoll, H.; Stone, A. J.; Tarroni, R.; Thorsteinsson, T.; Werner, H.-J. 2002.
(23) Peterson, K. A.; Woon, D. E.; Dunning, T. H., Jr. *J. Chem. Phys.* **1994**, *100*, 7410.
(24) Helgaker, T.; Klopper, W.; Koch, H.; Noga, J. *J. Chem. Phys.* **1997**, *106*, 9639.
(25) Halkier, A.; Helgaker, T.; Jørgensen, P.; Klopper, W.; Koch, H.; Olsen, J.; Wilson, A. K. *Chem. Phys. Lett.* **1998**, *286*, 243.
(26) Klopper, W.; Bak, K. L.; Jorgensen, P.; Olsen, J.; Helgaker, T. *J. Phys. B* **1999**, *32*, R103.
(27) Yabushita, S.; Zhang, Z.; Pitzer, R. M. *J. Phys. Chem. A* **1999**, *103*, 5791.
(28) Lischka, H.; Shepard, R.; Brown, F. B.; Shavitt, I. *Int. J. Quantum Chem. Symp.* **1981**, *15*, 91.
(29) Shepard, R.; Shavitt, I.; Pitzer, R. M.; Comeau, D. C.; Pepper, M.; Lischka, H.; Szalay, P. G.; Ahlrichs, R.; Brown, F. B.; Zhao, J. G. *Int. J. Quantum Chem. Symp.* **1988**, *22*, 149.

(30) Lischka, H.; Shepard, R.; Pitzer, R. M.; Shavitt, I.; Dallos, M.; Muller, T.; Szalay, P. G.; Seth, M.; Kedziora, G. S.; Yabushita, S.; Zhang, Z. *Phys. Chem. Chem. Phys.* **2001**, *3* (5), 664.

(31) Lischka, H.; Shepard, R.; Shavitt, I.; Pitzer, R. M.; Dallos, M.; Müller, T.; Szalay, P. G.; Brown, F. B.; Ahlrichs, R.; Böhm, H. J.; Chang, A.; Comeau, D. C.; Gdanitz, R.; Dachsel, H.; Ehrhardt, C.; Ernzerhof, M.; Höchtl, P.; Irle, S.; Kedziora, G.; Kovar, T.; Parasuk, V.; Pepper, M. J. M.; Scharf, P.; Schiffer, H.; Schindler, M.; Schüler, M.; Seth, M.; Stahlberg, E. A.; Zhao, J.-G.; Yabushita, S.; Zhang, Z.; COLUMBUS, an ab initio electronic structure program, release 5.8, 2001.

(32) Murrell, J. N.; Carter, S. *J. Chem. Phys.* **1984**, *88*, 4887.

(33) Ho, T.-S.; Rabitz, H. *J. Chem. Phys.* **1996**, *104*, 2584.

(34) Ho, T.-S.; Hollebeek, T.; Rabitz, H.; Chao, S. D.; Skodje, R. T.; Zyubin, A. T.; Mebel, A. M. *J. Chem. Phys.* **2002**, *116*, 4124.

(35) Murrell, J. N.; Carter, S.; Farantos, S. C.; Huxley, P.; Varandas, A. J. C. *Molecular Potential Energy Functions*; John Wiley and Sons: Chichester, U.K., 1984.

(36) Senekowitsch, J. Ph.D. Thesis, Universität Frankfurt, Frankfurt, Germany, 1988.

(37) Hollebeek, T.; Ho, T.-S.; Rabitz, H. *J. Chem. Phys.* **1997**, *106*, 7223.

(38) Corchado, J. C.; Chuang, Y.-Y.; Fast, P. L.; Villà, J.; Hu, W.-P.; Liu, Y.-P.; Lynch, G. C.; Nguyen, K. A.; Jackels, C. F.; Melissas, V. S.; Lynch, B. J.; Rossi, I.; Coitiño, E. L.; Fernandez-Ramos, A.; Pu, J.; Steckler, R.; Garrett, B. C.; Isaacson, A. D.; Truhlar, D. G. POLYRATE-version 8.7.2; University of Minnesota: Minneapolis, MN, 2002.

(39) Hase, W. L.; Duchovic, R. J.; Hu, X.; Komornicki, A.; Lim, K. F.; Lu, D.-h.; Peslherbe, G. H.; Swamy, K. N.; Vande Linde, S. R.; Varandas, A.; Wang, H.; Wolf, R. J. *Quantum Chemistry Program Exchange* **1996**, *16*, 671.

(40) Duchovic, R. J.; Volobuev, Y. L.; Lynch, G. C.; Truhlar, D. G.; Allison, T. C.; Wagner, A. F.; Garrett, B. C.; Corchado, J. C. *Comput. Phys. Commun.* **2002**, *144*, 169.

(41) Varandas, A. J. C. *Chem. Phys. Lett.* **1987**, *138* (5), 455.

(42) Mead, C. A.; Truhlar, D. G. *J. Chem. Phys.* **1979**, *70*, 2284.

(43) Wilcomb, B. E.; Haberman, J. A.; Bickes, R. W., Jr.; Mayer, T. M.; Bernstein, R. B. *J. Chem. Phys.* **1976**, *64*, 3501.

(44) Balabanov, N. B.; Peterson, K. A. *J. Phys. Chem. A* **2003**, *107*, 7465.

(45) Balabanov, N. B.; Peterson, K. A. *J. Chem. Phys.* **2003**, *119*, 12271.

(46) Peslherbe, G. H.; Wang, H.; Hase, W. L. *Adv. Chem. Phys.* **1999**, *105*, 171.

(47) Garrett, B. C.; Truhlar, D. G. *J. Phys. Chem.* **1979**, *83*, 1052.

(48) Garrett, B. C.; Truhlar, D. G.; Grev, R. S. In *Potential Energy Surfaces and Dynamics* Calculations; Truhlar, D. G., Ed.; Plenum: New York, 1980; p 587.

(49) Garrett, B. C.; Truhlar, D. G.; Grev, R. S.; Magnuson, A. W. *J. Phys. Chem.* **1980**, *84*, 1730.

(50) Garrett, B. C.; Truhlar, D. G.; Grev, R. S.; Magnuson, A. W. *J. Phys. Chem.* **1983**, *87*, 4554.

(51) Isaacson, A. D.; Truhlar, D. G. *J. Chem. Phys.* **1982**, *76*, 1380.

(52) Truhlar, D. G.; Isaacson, A. D.; Garrett, B. C. In *Theory of Chemical Reaction Dynamics*; Baer, M., Ed.; CRC Press: Boca Raton, FL, 1985; Vol. 4; p 65.

(53) Tucker, S. C.; Truhlar, D. G. In *New Theoretical Concepts for Understanding Organic Reactions*; Bertran, J., Csizmadia, I. G., Eds.; Kluwer: Dordrecht, The Netherlands, 1989.

(54) Steinfeld, J. I.; Francisco, J. S.; Hase, W. L. *Chemical Kinetics and Dynamics*; Prentice Hall: Englewood Cliffs, NJ, 1989.

(55) Calvert, J. G.; Lindberg, S. E. *Atmos. Environ.* **2003**, *37*, 4467.

(56) Calvert, J. G.; Lindberg, S. E. *Atmos. Environ.* **2004**, *38*, 5105.

(57) Tossel, J. A. *J. Phys. Chem. A* **2003**, *107*, 7804.

(58) Sheu, G.-R.; Mason, R. P. *J. Atmos. Chem.* **2004**, *48*, 107.

(59) Raofie, F.; Ariya, P. A. *J. Phys. IV* **2003**, *107*, 1119.

(60) Raofie, F.; Ariya, P. A. *Environ. Sci. Technol.* **2004**, *38*, 4319.

(61) Shepler, B. C.; Peterson, K. A. *J. Phys. Chem. A* **2003**, *107*, 1783.

(62) Focsa, C.; Li, H.; Bernath, P. F. *J. Mol. Spectrosc.* **2000**, *200* (1), 104.

(63) Tellinghuisen, J.; Ashmore, J. G. *Appl. Phys. Lett.* **1982**, *40*, 867.

(64) Chase, M. W., Jr.; Davies, C. A.; Downey, J. R., Jr.; Frurip, D. J.; McDonald, R. A.; Syverud, A. N. *J. Phys. Chem. Ref. Data* **1985**, *14*, Suppl. No. 1.

(65) Tellinghuisen, J.; Ashmore, J. G. *Chem. Phys. Lett.* **1983**, *102* (1), 10.